

Magnetic vector constraint pedestrian dead reckoning based on foot-mounted and waist-mounted IMU

Jian Kuang, Tao Liu, Yan Wang, Xianmei Meng and Xiaoji Niu

Abstract—The foot-mounted inertial navigation system (Foot-INS) is a crucial technology for professional pedestrian positioning, unaffected by environmental conditions. However, due to the unobservable nature of the absolute heading, single or dual Foot-INS configurations suffer from significant position drift errors. This paper introduces an innovative pedestrian dead reckoning (PDR) method that combines foot-mounted and waist-mounted IMU with magnetic field vector constraints. Leveraging the fact that the displacements of the foot and waist are consistent when the foot makes ground contact, the proposed method uses the relative displacement estimated by Foot-INS to correct the waist-mounted INS. Building on this, a relative magnetic field vector constraint method is developed using error state clonal Kalman filtering, capitalizing on the similarity of magnetic interference within a local area. The results from 12 tests conducted in typical indoor environments, such as offices and underground parking lots, demonstrate that the proposed method significantly enhances positioning performance in areas with frequent magnetic interference. The positioning error is reduced by more than 49% compared to single or dual Foot-INSs.

Index Terms—Pedestrian dead reckoning (PDR), foot-mounted inertial navigation system (Foot-INS), magnetic field, pedestrian navigation.

I. INTRODUCTION

PEDESTRIAN navigation system (PNS) is a critical technology for safeguarding workers' lives in indoor environments, such as factory personnel safety monitoring, fire rescue and emergency search [1], [2], [3], [4]. Sensor-based PNS is a prevalent solution for professional indoor pedestrian localization as it does not depend on prior information, such as signal base stations and signal fingerprints. High-precision sensor-based PNS schemes typically employ LiDAR [5], vision [6], and inertial measurement units (IMUs) [7], [8]. Unlike LiDAR and camera systems, which achieve positioning by observing the surrounding environment, IMU-based PNS relies solely on observed motion information. This

autonomous positioning method is unaffected by external environmental factors. Moreover, micro-electromechanical system IMU (MEMS-IMU) based PNS has become an indispensable technology for most PNS solutions due to its advantages of low cost, low power consumption, and compact size [9], [10], [11], [12].

High-precision pedestrian navigation systems (PNS) based on MEMS-IMU typically refer to foot-mounted inertial navigation systems (Foot-INS). Foot-INS operates on the assumption that a pedestrian's feet periodically make contact with the ground, utilizing zero-velocity update technology (ZUPT) to control the velocity error of inertial navigation, thus achieving stable relative position estimation [13]. However, the heading of Foot-INS is not appreciable or is weakly appreciable when only ZUPT is available [14]. To enhance the accuracy and reliability of Foot-INS, multi-constraint correction algorithms have been developed [15], [16]. Zero Integrated Heading Rate (ZIHR) assumes that the change in heading during foot contact are due to sensor error, and is only suitable for users who remain stationary for extended periods. Straight-line constraints rely on the user's tendency to walk in straight-line trajectories, constructing heading-invariant observations to control heading drift. On this basis, the heuristic heading reduction extracts building orientation to create a heading fingerprint, effectively controlling heading errors over the long term [17]. However, its effectiveness, as well as that of straight-line constraints, depends on the walking trajectory's shape and may be limited in complex environments. By observing the geomagnetic field, the compass provides very accurate and reliable heading information for Foot-INS in outdoor scenes. Nevertheless, it faces usability challenges indoors due to magnetic interference from ferromagnetic objects. These improved heading estimation methods are only suitable for specific user dynamics and positioning environments. In complex scenes, such as irregular indoor spaces, the positioning performance of Foot-INS still deteriorates significantly [18].

PNS based on two or more sensors can enhance the state observability of the heading and sensor noises (e.g., gyroscope biases) [19], [20], such as the dual-foot-based PNS and the body-sensor-network-based PNS. The dual-foot-based PNS installs two MEMS-IMUs on the left and right foot, respectively, providing a theoretical double correction opportunity for zero-velocity information compared to the single-foot solution. By leveraging the regular and periodic constraints between the left and right feet during walking, the system reduces the position error divergence [19]. The core concept of dual-

This work was supported in part by the Hubei Provincial Natural Science Foundation Program under Grant 2023AFB021, in part by the Fundamental Research Funds for the Central Universities (2042023kf0124). (Corresponding author: Yan Wang.)

J. Kuang, Y. Wang and X. Niu are with the GNSS Research Center, Wuhan University, Wuhan, Hubei, CO 430072 PR China. X. Niu is also with the Collaborative Innovation Center of Geospatial Technology, Wuhan University. (E-mails: kuang@whu.edu.cn; wstephen@whu.edu.cn; xjniu@whu.edu.cn.)

T. Liu is with the School of Software, Jiangxi Normal University, Nanchang, Jiangci, CO 330022 PRChina. (Email: liu_tao@jxnu.edu.cn.)

X. Meng is with the School of Nursing, Wuhan University, Wuhan, Hubei, CO 430072 PRChina. (Email: hopemengmei@163.com.)

foot-based PNS is to use the distance between the feet to establish a link, which can be implemented with or without an additional ranging sensor [14]. In the ranging-sensor-based solution, a pair of ultrasonic sensors [21] or visual devices [22], are used to measure the distance between the feet. In the dual-foot solution without the assistance of a ranging sensor, the maximum distance constraint is the most classic approach, assuming a maximum separation between the feet [23]. However, the minimum distance between feet is relatively constant in most walking scenarios [24]. Therefore, our previous work proposed a minimum distance constraint approach, which has demonstrated superior positioning performance and robustness compared to the maximum distance constraint method [25]. Dual-foot-based PNS offers strong autonomous positioning capability and robustness. However, accurately estimating heading and position remains challenging, causing pedestrian positioning errors to still increase over time.

Compared to PNS based on foot-mounted IMUs, PNS systems that use IMUs installed in other parts of the body typically exhibit lower positioning performance due to the absence of zero-velocity updates. However, these systems benefit from significantly reduced magnetic interference at the waist and above. Body-sensor-network-based PNS takes advantage of the distinct characteristics of multiple sensors placed on the body to achieve more accurate positioning. A classical approach involves transferring the foot position data to the waist and using it as an independent observation. This data is then combined with compass to correct the navigation state of the waist-mounted INS [26], [27]. However, the position estimated by Foot-INS is divergent rather than convergent, and the position error cannot be modeled as zero-mean Gaussian white noise. Consequently, this method does not fully leverage the advantages of multi-sensor fusion, resulting in limited improvements in positioning performance. Moreover, waist-mounted magnetometers in indoor environments still suffer from significant magnetic interference. While the quasi-static magnetic field (QSF) technique can effectively use magnetometer measurements to estimate heading in highly perturbed environments, the stochastic nature of stable magnetic field regions in the environment limits the effectiveness of QSF [28], [29]. As a result, the heading estimation can still diverge quickly. In summary, although body-sensor-network-based PNS can reduce some magnetic interference and potentially improve positioning through multi-sensor fusion, challenges such as divergence in foot position estimates and magnetic interference in indoor environments limit the overall effectiveness and accuracy of these systems.

In this study, we present a magnetic vector constraint pedestrian dead reckoning system that integrates a foot-mounted IMU and a waist-mounted IMU. The core idea is to use Waist-INS as an information bridge, integrating the high-precision relative displacement provided by Foot-INS and the heading constraint provided by the magnetic vector to achieve more reliable pedestrian position estimation. Leveraging the objective fact that the position increments of the foot and waist are consistent between two consecutive foot-ground contact periods, the position increment generated by Foot-INS is used as an independent observation to correct Waist-INS.

We utilize state cloning Kalman filtering to fuse the Waist-INS data with magnetic field vectors within a time window (e.g., 20 seconds). This approach suppresses the influence of magnetic interference by using differential magnetic field vectors, thereby effectively reducing the position error caused by heading drift.

The remainder of the paper is organized as follows: Section II provides an overview of the proposed system. Section III describes the basic concept of Foot-INS and the estimation of relative position increments. Section IV introduces a waist-mounted INS with magnetic vector constraints. Section V presents the experimental results. Section VI summarizes the key findings of the study.

II. SYSTEM OVERVIEW

Foot-INS can accurately estimate a user's displacement under complex pedestrian gaits because it does not rely on strict motion model assumptions, such as assuming people only walk in the direction they are facing. On the other hand, Waist-mounted INS (Waist-INS) is less susceptible to magnetic interference and can use magnetometer observations to obtain more accurate heading estimates. Therefore, it is natural to consider fusing Foot-INS and Waist-INS to achieve higher positioning estimation performance than either algorithm can provide individually.

Figure 1 illustrates the relative position relationship between the waist and the foot throughout a gait cycle, which can be simplified into four stages (H1, H2, H3, and H4). The dynamics of the foot are significantly greater than those of the waist, and the relative positional relationship between them is not fixed. However, there are periodic instances, such as when the foot (with the IMU) supports the forward movement of the pedestrian's body (e.g., stages H1 or H3), where the projections of the foot and waist on the ground coincide. Traditional methods utilize these periodic phenomena to construct distance constraints for fusing Foot-INS and Waist-INS, but this approach typically achieves positioning performance similar to that of Foot-INS alone [30]. Therefore, this paper proposes using Foot-INS as a sensor to observe relative displacement (specifically, extracting the position change at adjacent H1 stages) to correct the navigation state of Waist-INS.

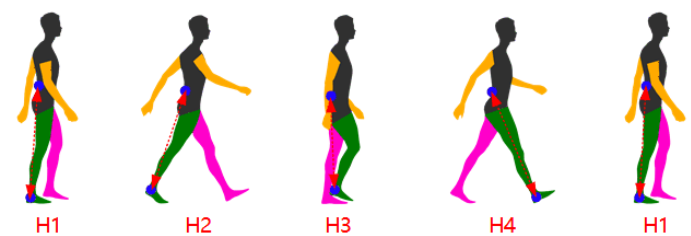


Fig. 1. The relative position of the waist and foot in a step cycle.

Figure 2 shows the block diagram of the proposed PDR algorithm. The proposed method employs a state cloning extended Kalman filter (SC-EKF) to integrate Waist-INS, Foot-INS, and magnetic field data. Foot-INS serves as the

displacement measurement sensor within the algorithm, ensuring accurate estimation of the user's position increments. Additionally, the relative change of the magnetic field within a sliding window is utilized to mitigate the impact of magnetic interference and effectively suppress heading drift errors.

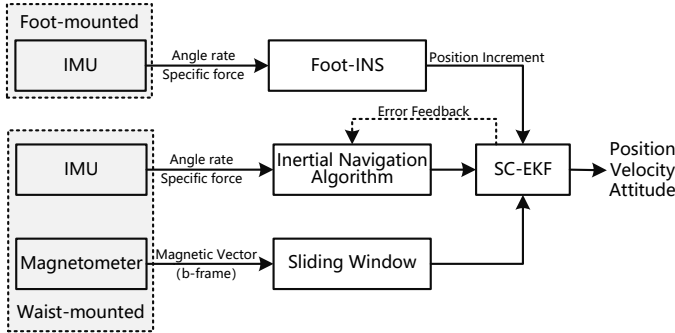


Fig. 2. Block diagram of the proposed PDR algorithm based on a foot-mounted IMU and a waist-mounted IMU.

III. FOOT-MOUNTED INS

Compared to step-model-based pedestrian dead reckoning (PDR), Foot-INS is more versatile because it directly senses the user's dynamics to estimate position changes. Unfortunately, its heading estimation tends to diverge rapidly due to the lack of effective observations. Previous studies [18] often restrict the user's walking trajectory shape (e.g., assuming straight-line trajectories) and the environment (e.g., office corridors) to improve Foot-INS positioning performance. However, this approach can lead to significant differences in positioning accuracy across different users and environments.

Foot-INS utilizes the well-known generalized likelihood ratio detector [14] to identify periods when the foot is in contact with the ground, performing zero-velocity updates during the static period. A 15-dimensional system state is employed, encompassing position error, velocity error, attitude error, gyroscope bias, and accelerometer bias. To minimize dependency on specific user motion trajectories and positioning environments, this paper implements Foot-INS solely with ZUPT. For detailed algorithmic specifics, refer to [15].

Based on the objective observation that when the IMU is installed on the foot to support the pedestrian's forward movement, the projections of the foot and waist on the ground coincide periodically, this paper utilizes the foot-mounted INS as an independent odometer. It extracts sparse position increments from the continuous position output by Foot-INS. These low-frequency position increments can be represented as:

$$\Delta \mathbf{r}_{k,i}^f = \mathbf{r}_k^f - \mathbf{r}_i^f \quad (1)$$

where \mathbf{r}^f is the position vector in the f -frame, f -frame represents the navigation frame estimated by Foot-INS, k and i are the data epochs corresponding to two adjacent steps, and the steps refer to the epoch corresponding to the middle moment in the static period.

Based on the conclusion from Reference [14], the position estimated by Foot-INS is strongly correlated with heading

only under the assumption of zero velocity. Building upon this, Equation 1 eliminates absolute heading by subtracting the positions of adjacent footsteps. This process ensures that the resulting position increment observation is independent of historical navigation states. In other words, the displacement increment observation adheres to the assumption in filtering that observations follow Gaussian white noise.

IV. WAIST-MOUNTED INS WITH MAGNETIC VECTOR CONSTRAINT

In this section, we outline the fusion algorithm for integrating Foot-INS and Waist-INS. The output from the waist-mounted IMU is utilized for integral calculations to derive current position, velocity, and attitude. Concurrently, relative position increments from the Foot-INS are extracted to effectively mitigate position drift using the State Clone Extended Kalman Filter (SC-EKF). Additionally, the incremental changes in the magnetic field vector within the n -frame are incorporated to enhance the estimation accuracy of the position.

A. Inertial Navigation Algorithm

INS mechanization is a fundamental algorithm in inertial navigation, characterized by a rigorous theoretical framework. Due to the limitations of MEMS-IMUs, which are low quality and prone to errors, certain corrections, such as those related to Earth's rotation, are often omitted because they do not yield significant performance improvements. The simplified INS mechanization is described by [31]:

$$\mathbf{r}_k^n = \mathbf{r}_{k-1}^n + \mathbf{v}_k^n \Delta t_k \quad (2)$$

$$\mathbf{v}_k^n = \mathbf{v}_{k-1}^n + \mathbf{C}_{b,k}^n \left(\Delta \mathbf{v}_k^b + \frac{\Delta \boldsymbol{\theta}_k^b \times \Delta \mathbf{v}_k^b}{2} \right) + \mathbf{g}^n \Delta t_k \quad (3)$$

$$\mathbf{C}_{b,k}^n = \mathbf{C}_{b,k-1}^n \left[\mathbf{I} + \Delta \boldsymbol{\theta}_k^b + \frac{\Delta \boldsymbol{\theta}_{k-1}^b \times \Delta \boldsymbol{\theta}_k^b}{12} \right] \quad (4)$$

where \mathbf{r}^n and \mathbf{v}^n are the position and velocity vectors in the n -frame, respectively; \mathbf{C}_b^n is the transformation matrix from the b -frame to the n -frame; $\mathbf{g}^n = [0, 0, -9.8]^T$ is Earth's gravity vector; $\Delta \mathbf{v}_k^b = (\tilde{\mathbf{a}}_k^b - \mathbf{b}_{a,k}) \Delta t_k$ is the velocity increment in the b -frame; $\tilde{\mathbf{a}}^b$ and \mathbf{b}_a are the acceleration and bias of the accelerometer, respectively; $\Delta \boldsymbol{\theta}_k^b = (\tilde{\boldsymbol{\omega}}_k^b - \mathbf{b}_{\omega,k}) \Delta t_k$ is the angle increment in the b -frame; $\tilde{\boldsymbol{\omega}}^b$ and \mathbf{b}_g are the angle rate and bias of the gyroscope, respectively; $\Delta t_k = t_k - t_{k-1}$ is the time interval between the $(k-1)$ -th and k -th epochs; and " \times " is the cross-product form of a vector.

B. State Clone Extended Kalman Filter

In the proposed algorithm, a SC-EKF is employed to fuse the relative position increments of the two IMUs. Additionally, the incremental changes in the magnetic field vector are utilized to enhance heading estimation performance, thereby further improving overall position estimation accuracy.

The system utilizes an error-state-based indirect SC-EKF approach, where the error state represents the difference between estimated and actual values. At time k , the $(22+3 \times m)$ -dimensional error state variables are defined as:

$$\delta \mathbf{x}_k = \begin{bmatrix} \mathbf{s}_k & \boldsymbol{\eta}_i \end{bmatrix} \quad (5)$$

where

$$\boldsymbol{\eta}_i = [\delta \mathbf{r}_i^n \quad \boldsymbol{\phi}_{i-m} \quad \boldsymbol{\phi}_{i-m+1} \quad \cdots \quad \boldsymbol{\phi}_i]^T,$$

$$\mathbf{s}_k = [\delta \mathbf{r}_k^n \quad \delta \mathbf{v}_k^n \quad \boldsymbol{\phi}_k \quad \delta \mathbf{b}_{g,k} \quad \delta \mathbf{b}_{a,k} \quad \delta \mathbf{b}_{m,k} \quad \delta \alpha_k]^T,$$

$\delta \mathbf{r}^n$ and $\delta \mathbf{v}^n$ are the position and velocity error vectors in the n -frame, respectively; $\boldsymbol{\phi}$ is the attitude error vector; $\delta \mathbf{b}_g$, $\delta \mathbf{b}_a$ and $\delta \mathbf{b}_m$ are the bias error vectors of the gyroscope, accelerometer and magnetometer, respectively; and $\delta \alpha$ is the angle difference error between the f -frame maintained by foot-INS and the n -frame maintained by waist-INS, the subscript "i" is the cloned state at time i, including the 3D position and attitude, "m" is the length of the sliding window.

In the SC-EKF, the cloned states do not require updating during the propagation stage. The propagation of the error-state covariance can be expressed as:

$$\mathbf{P}_k = \boldsymbol{\Phi}_k \mathbf{P}_{k-1} \boldsymbol{\Phi}_k^T + \mathbf{G}_k \mathbf{Q} \mathbf{G}_k^T \quad (6)$$

where

$$\boldsymbol{\Phi}_k = \begin{bmatrix} \boldsymbol{\Phi}_k^s & \mathbf{0}_{19 \times (3+3m)} \\ \mathbf{0}_{(3+3m) \times 19} & \mathbf{I}_{3+3m} \end{bmatrix}, \mathbf{G}_k = \begin{bmatrix} \mathbf{G}_k^s \\ \mathbf{0}_{3+3m} \end{bmatrix},$$

$$\boldsymbol{\Phi}_k^s = \begin{bmatrix} \mathbf{I}_3 & \boldsymbol{\Phi}_{12} & \mathbf{0}_3 & \mathbf{0}_3 & \mathbf{0}_3 & \mathbf{0}_3 & \mathbf{0}_{3 \times 1} \\ \mathbf{0}_3 & \mathbf{I}_3 & \boldsymbol{\Phi}_{23} & \mathbf{0}_3 & \boldsymbol{\Phi}_{25} & \mathbf{0}_3 & \mathbf{0}_{3 \times 1} \\ \mathbf{0}_3 & \mathbf{0}_3 & \mathbf{I}_3 & \boldsymbol{\Phi}_{34} & \mathbf{0}_3 & \mathbf{0}_3 & \mathbf{0}_{3 \times 1} \\ \mathbf{0}_3 & \mathbf{0}_3 & \mathbf{0}_3 & \mathbf{I}_3 & \mathbf{0}_3 & \mathbf{0}_3 & \mathbf{0}_{3 \times 1} \\ \mathbf{0}_3 & \mathbf{0}_3 & \mathbf{0}_3 & \mathbf{0}_3 & \mathbf{I}_3 & \mathbf{0}_3 & \mathbf{0}_{3 \times 1} \\ \mathbf{0}_3 & \mathbf{0}_3 & \mathbf{0}_3 & \mathbf{0}_3 & \mathbf{0}_3 & \mathbf{I}_3 & \mathbf{0}_{3 \times 1} \\ \mathbf{0}_{1 \times 3} & 1 \end{bmatrix},$$

$$\mathbf{G}_k^s = \begin{bmatrix} \mathbf{0}_3 & \mathbf{0}_3 & \mathbf{0}_3 & \mathbf{0}_3 & \mathbf{0}_3 & \mathbf{0}_{3 \times 1} \\ \mathbf{C}_b^n & \mathbf{0}_3 & \mathbf{0}_3 & \mathbf{0}_3 & \mathbf{0}_3 & \mathbf{0}_{3 \times 1} \\ \mathbf{0}_3 & -\mathbf{C}_b^n & \mathbf{0}_3 & \mathbf{0}_3 & \mathbf{0}_3 & \mathbf{0}_{3 \times 1} \\ \mathbf{0}_3 & \mathbf{0}_3 & \mathbf{I}_3 & \mathbf{0}_3 & \mathbf{0}_3 & \mathbf{0}_{3 \times 1} \\ \mathbf{0}_3 & \mathbf{0}_3 & \mathbf{0}_3 & \mathbf{I}_3 & \mathbf{0}_3 & \mathbf{0}_{3 \times 1} \\ \mathbf{0}_3 & \mathbf{0}_3 & \mathbf{0}_3 & \mathbf{0}_3 & \mathbf{I}_3 & \mathbf{0}_{3 \times 1} \\ \mathbf{0}_{3 \times 1} & 1 \end{bmatrix},$$

$\boldsymbol{\Phi}_k^s$ and \mathbf{G}_k^s are the linearized state propagation matrix of the previous state $\hat{\mathbf{s}}_{t-1}$ and all noise (including sensor noise and biased random walk noise), respectively. $\boldsymbol{\Phi}_{12} = \mathbf{I}_3 \Delta t_k$, $\boldsymbol{\Phi}_{23} = (\mathbf{f}_k^n \times) \Delta t_k$, $\boldsymbol{\Phi}_{25} = \mathbf{C}_{b,k}^n \Delta t_k$, $\boldsymbol{\Phi}_{34} = -\mathbf{C}_{b,k}^n \Delta t_k$, \mathbf{I}_3 is a 3-dimension identity matrix.

When the observations are valid, the following methods can be used to update the state variables and their corresponding covariance [25]:

$$\delta \hat{\mathbf{x}}_k = \delta \hat{\mathbf{x}}_{k,k-1} + \mathbf{K}_k (\delta \mathbf{z}_k - \mathbf{H}_k \hat{\mathbf{x}}_{k,k-1}) \quad (7)$$

$$\mathbf{P}_k = (\mathbf{I} - \mathbf{K}_k \mathbf{H}_k) \mathbf{P}_{k,k-1} (\mathbf{I} - \mathbf{K}_k \mathbf{H}_k)^T + \mathbf{K}_k \mathbf{R}_k \mathbf{K}_k^T \quad (8)$$

$$\mathbf{K}_k = \mathbf{P}_{k,k-1} \mathbf{H}_k^T (\mathbf{H}_k \mathbf{P}_{k,k-1} \mathbf{H}_k^T + \mathbf{R}_k)^{-1} \quad (9)$$

The measurement update of the SC-EKF incorporates the relative position and relative attitude between the current system state and a previous system state. To maintain continuity, the previous system state (i.e., \mathbf{r}^n and $\boldsymbol{\phi}$) is retained in the SC-EKF through stochastic cloning. The cloned system state is an exact replica of the current system state, focusing solely

on \mathbf{r}_t^n and $\boldsymbol{\phi}_t$. The probability propagation of the stochastic clone step in the proposed system is defined as:

$$\mathbf{P}_k^{new} = \begin{bmatrix} \mathbf{I}_{19} & \mathbf{0}_{19 \times (3+3m)} \\ \mathbf{A} & \mathbf{A} \end{bmatrix} \mathbf{P}_k \begin{bmatrix} \mathbf{I}_{19} & \mathbf{0}_{19 \times (3+3m)} \\ \mathbf{A} & \mathbf{A} \end{bmatrix}^T \quad (10)$$

$$\mathbf{A} = \begin{bmatrix} \mathbf{I}_3 & \mathbf{0}_3 & \mathbf{0}_3 & \mathbf{0}_{3 \times 13} & \mathbf{0}_3 & \cdots & \mathbf{0}_3 \\ \mathbf{0}_3 & \mathbf{0}_3 & \mathbf{0}_3 & \mathbf{0}_{3 \times 13} & \mathbf{I}_3 & \cdots & \mathbf{0}_3 \\ \vdots & \vdots & \vdots & \vdots & \vdots & \vdots & \vdots \\ \mathbf{0}_3 & \mathbf{0}_3 & \mathbf{I}_3 & \mathbf{0}_{3 \times 13} & \mathbf{0}_3 & \cdots & \mathbf{0}_3 \end{bmatrix} \quad (11)$$

where the rows and columns of \mathbf{A} are $(3 + 3 \times m)$ and $(22 + 3 \times m)$.

C. Position Increment Update

Although there is significant dynamic difference between the foot and the waist during walking, the position increments measured by Foot-INS and Waist-INS between two adjacent steps are consistent. This phenomenon can be expressed as:

$$\mathbf{0} = \mathbf{r}_k^n - \mathbf{r}_i^n - \mathbf{C}_f^n \Delta \mathbf{r}_{k,i}^f \quad (12)$$

where \mathbf{r}^n represents the position estimated by Waist-INS at epochs k and i , respectively. In the initialization phase, \mathbf{C}_f^n (the direction cosine matrix from the f -frame to the n -frame) is assumed to be the unit matrix, indicating that the f -frame and n -frame are parallel. However, due to inconsistent heading drift rate between Foot-INS and waist-mounted INS over time, \mathbf{C}_f^n varies as time progresses. Perturbation analysis of the Eq. 12 can be expressed as follows:

$$\begin{aligned} \delta \mathbf{z}_{\Delta \mathbf{r}_{k,i}^n} &= (\hat{\mathbf{r}}_k^n - \hat{\mathbf{r}}_i^n) - \hat{\mathbf{C}}_f^n \Delta \tilde{\mathbf{r}}_{k,i}^f \\ &= (\mathbf{r}_k^n + \delta \mathbf{r}_k^n) - (\mathbf{r}_i^n + \delta \mathbf{r}_i^n) \\ &\quad - (\mathbf{I} - \boldsymbol{\kappa} \times) \mathbf{C}_f^n \left(\Delta \mathbf{r}_{k,i}^f + \mathbf{n}_{\Delta \mathbf{r}_{k,i}^f} \right) \\ &= \left(\Delta \mathbf{r}_{k,i}^n - \mathbf{C}_f^n \Delta \mathbf{r}_{k,i}^f \right) + \delta \mathbf{r}_k^n - \delta \mathbf{r}_i^n \\ &\quad - \left(\mathbf{C}_f^n \Delta \mathbf{r}_{k,i}^f \right) \times \boldsymbol{\kappa} - \mathbf{C}_f^n \mathbf{n}_{\Delta \mathbf{r}_{k,i}^f} \end{aligned} \quad (13)$$

where $\Delta \mathbf{r}_{k,i}^n = \mathbf{r}_k^n - \mathbf{r}_i^n$ represents the position increment predicted by Waist-INS; $\boldsymbol{\kappa} = [0 \quad 0 \quad \delta \alpha]^T$, $\mathbf{C}_f^n = \begin{bmatrix} \cos \alpha & \sin \alpha & 0 \\ \sin \alpha & \cos \alpha & 0 \\ 0 & 0 & 1 \end{bmatrix}$ represents the direction cosine matrix between f -frame and n -frame; $\mathbf{n}_{\Delta \mathbf{r}_{k,i}^f}$ represents the noise for position increments given by Foot-INS. $\boldsymbol{\kappa} \times \mathbf{C}_f^n \mathbf{n}_{\Delta \mathbf{r}_{k,i}^f}$ is neglected because it is a small second-order error. The corresponding observation matrix can be expressed as:

$$\mathbf{H}_{\Delta \mathbf{r}^n} = \begin{bmatrix} \mathbf{I}_3 & \mathbf{0}_{3 \times 15} & \left[- \left(\mathbf{C}_f^n \Delta \mathbf{r}_{k,i}^f \right) \times \right]_{(:,3)} & -\mathbf{I}_3 & \mathbf{0}_{3 \times 3m} \end{bmatrix}^T \quad (14)$$

When the pedestrian is standing still, the position error can be controlled using a zero position increment observation. This observation equation is expressed as:

$$\mathbf{0} = \hat{\mathbf{r}}_k^n - \hat{\mathbf{r}}_i^n \quad (15)$$

The corresponding observation matrix can be expressed as:

$$\mathbf{H}_{\Delta \mathbf{r}^n} = \begin{bmatrix} \mathbf{I}_3 & \mathbf{0}_{3 \times 16} & -\mathbf{I}_3 & \mathbf{0}_{3 \times 3m} \end{bmatrix}^T \quad (16)$$

D. Magnetic Vector Constraint Update

Without considering the scale factor and non-orthogonal error, the simplified magnetometer observation model can be described as [32]:

$$\tilde{M}^b = C_n^b (M_G^n + M_I^n) + \mathbf{b}_m + \mathbf{n}_m \quad (17)$$

where M_G^n and M_I^n are the geomagnetic field and magnetic field interference in the n -frame, respectively; \tilde{M}^b and \mathbf{b}_m are the measurement and bias of magnetometer, respectively; C_n^b is the transformation matrix from the n -frame to the b -frame; \mathbf{n}_m is the measurement noise. The geomagnetic field at time k can be expressed as:

$$M_{G,k}^n = C_{b,k}^n (\tilde{M}_k^b - \mathbf{b}_{m,k}) + M_{I,k}^n + C_{b,k}^n \mathbf{n}_m \quad (18)$$

Since magnetic interference in typical indoor environments primarily originates from reinforced concrete structures, it is reasonable to assume that the magnetic field interference M_I^n during normal pedestrian walking scenes is a slowly varying variable. Figure 3 illustrates the magnetic field vectors observed in the local coordinate frame in an office scenario (The data collection trajectory is shown in Figure 5-(d)). Sub-figure (b) depicts the magnetic disturbance specific to this environment, while sub-figure (c) shows the differential magnetic field vector aimed at mitigating such disturbances. In sub-figure (b), the standard deviations of the magnetic vectors in each direction are 59.2 milligauss, 59.2 milligauss, and 71.3 milligauss, the standard deviations in sub-figure (c) are 17.1 milligauss, 13.6 milligauss, and 20.1 milligauss. This reduction indicates that the differential magnetic field vector can effectively diminish the impact of magnetic interference by more than 70%.

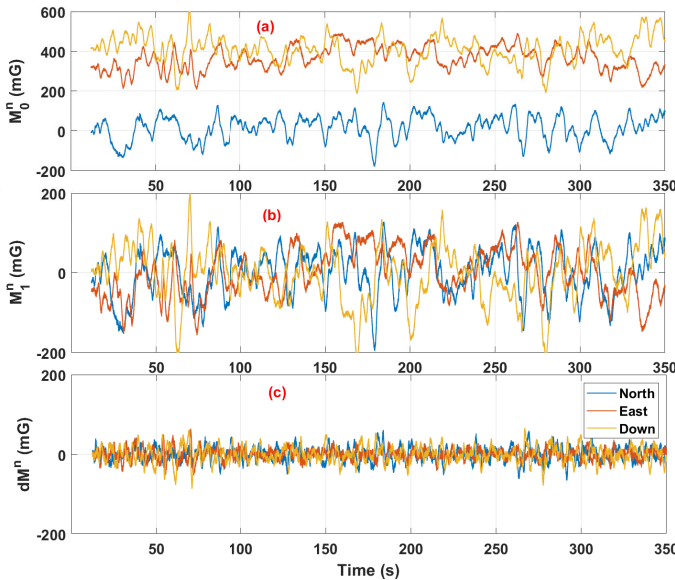


Fig. 3. Magnetic field vectors in the local coordinate frame observed in the underground parking scene. (a) Magnetic field vector $M_{0,i}^n = C_{b,i}^n (\tilde{M}_i^b - \mathbf{b}_m)$, (b) Magnetic field vector after deducting the mean $M_{1,i}^n = M_{0,i}^n - \frac{1}{k} \sum_{i=1}^k M_{0,i}^n$, (c) Difference of magnetic field vector at interval of 0.5 seconds $dM_i^n = M_{0,i+0.5}^n - M_{0,i}^n$.

Based on the property that the differential magnetic field vector can effectively suppress the influence of magnetic interference, we reasonably assume that the magnetic interference in a small area is approximately equal.

$$M_{G,1}^n \approx M_{G,2}^n \approx \dots \approx M_{G,k}^n \quad (19)$$

The magnetic field vector at any two moments in a small area satisfies the following equation.

$$\mathbf{0} \approx M_{G,k}^n - M_{G,i}^n \quad (20)$$

Substituting Eq. 18 into Eq. 20 gives

$$\mathbf{0} \approx C_{b,k}^n (\tilde{M}_k^b - \mathbf{b}_{m,k}) - C_{b,i}^n (\tilde{M}_i^b - \mathbf{b}_{m,i}) \quad (21)$$

The magnetometer bias can be considered as unchanged in a short period of time (e.g., 15 seconds) [10], and perturbation analysis of the Eq. 21 can be expressed as:

$$\begin{aligned} \delta z_{\Delta M_{k,i}^n} &= \hat{C}_{b,k}^n (\tilde{M}_k^b - \hat{\mathbf{b}}_{m,k}) - \hat{C}_{b,i}^n (\tilde{M}_i^b - \hat{\mathbf{b}}_{m,k}) \\ &= (\mathbf{I} - \phi_k \times) C_{b,k}^n (\tilde{M}_k^b - \mathbf{b}_{m,k} - \delta \mathbf{b}_{m,k}) \\ &\quad - (\mathbf{I} - \phi_i \times) C_{b,i}^n (\tilde{M}_i^b - \mathbf{b}_{m,k} - \delta \mathbf{b}_{m,k}) \\ &\approx \Delta M_{k,i}^n + M_k^n \times \phi_k - M_i^n \times \phi_i - (C_{b,k}^n - C_{b,i}^n) \delta \mathbf{b}_{m,k} \end{aligned} \quad (22)$$

where

$$\begin{aligned} \Delta M_{k,i}^n &= [C_{b,k}^n (\tilde{M}_k^b - \mathbf{b}_{m,k}) - C_{b,i}^n (\tilde{M}_i^b - \mathbf{b}_{m,k})], \\ M_k^n &= [C_{b,k}^n (\tilde{M}_k^b - \mathbf{b}_{m,k})], \\ M_i^n &= [C_{b,i}^n (\tilde{M}_i^b - \mathbf{b}_{m,k})]. \end{aligned}$$

The observation equation corresponding to the magnetic field vector between k -th and i -th epoch can be expressed as:

$$H_{\Delta M}^n = [\mathbf{0}_{3 \times 6} \quad M_k^n \times \quad \mathbf{0}_{3 \times 6} \quad C_{b,i}^n - C_{b,k}^n \quad \mathbf{0}_{3 \times 4} \quad M_i^n \times] \quad (23)$$

Since the indoor magnetic field anomaly has a random characteristic, the algorithm implementation will use the average value of the magnetic field vector in the window to replace the magnetic field vector observation at a certain moment.

V. EXPERIMENTAL RESULTS

A. Test Description

Figure V-A illustrates the positional arrangement of sensors worn by the tester, including a foot-mounted IMU, waist-mounted IMU, and LiDAR SLAM system. The foot-mounted IMU is located at the heel, while the waist-mounted IMU is positioned at the back waist. The x-axis of the waist-mounted IMU is roughly parallel to the pedestrian's forward direction (e.g., the angle should be less than 15°), which is an effective measure to ensure that the proposed method can quickly reach a convergence state. Additionally, a LiDAR SLAM system is installed in the backpack. The inertial module used in the experiment was developed by the WHU-i2Nav team and includes a MEMS IMU, power module, Bluetooth low energy module, memory module (SD card), and a powerful general-purpose multi-protocol system-on-chip (SoC). Time synchronization among multiple devices is achieved by

transmitting timestamps to smartphones via Bluetooth. The bias instability of the inertial sensors is $10^\circ/h$ and 0.2 mg , the white noise is $0.24^\circ/\sqrt{h}$ and $0.06\text{ m/s}/\sqrt{h}$. In typical indoor environments, the LiDAR SLAM system provides a position reference with centimeter-level accuracy (see Table I for specific parameters), which is essential for evaluating the performance of the positioning system. The reference attitude is calculated by combining the position output by LiDAR SLAM system with the waist-mounted IMU and then reversely smoothed.



Fig. 4. The relative positional relationship between foot-mounted IMU, waist-mounted IMU, and LiDAR SLAM.

TABLE I
SPECIFICATIONS OF THE LiDAR SLAM SYSTEM

Parameters	Value
Model	GoSlam RS100i
Measurement Accuracy	1 cm (Relative), 2 cm (Absolute)
Range	Up to 120 m
Scan Speed	320,000 points/second
Point Precision	2 mm (peak precision)
Operating Time	4 hours

We conducted a positioning performance evaluation involving five different schemes: 1) **L-Foot and R-Foot**: This scheme utilizes zero-velocity update (ZUPT), without incorporating additional observations such as linear constraints or magnetometer observations based on specific user motion trajectory shapes and positioning environments [15]. 2) **Dual-Foot**: Building upon L-Foot and R-Foot, this solution adds the constraint of the shortest distance between the left and right feet. For detailed methods, please refer to [25]. 3) **Heading-Step**: This scheme estimates step length using L-Foot and determines heading using an attitude and heading reference system (AHRS) as described in the literature [29]. 4) **Proposed**: The algorithms described in Sections III and IV of this paper. L-Foot is used to provide relative displacement increments..

In the initial stage, the position and velocity vectors of Waist-INS are set to zero, the roll and pitch are estimated

by the accelerometer observations, the heading of Foot-INS set to zero, and the heading of Waist-INS is estimated by the relative displacement output by Foot-INS. The details are as follows:

$$\begin{cases} \phi = \tan^{-1} \frac{-a_y^b}{-a_z^b} \\ \theta = \tan^{-1} \frac{a_x^b}{\sqrt{(a_y^b)^2 + (a_z^b)^2}} \\ \psi = \tan^{-1} \frac{\Delta r_{1,y}^f}{\Delta r_{1,x}^f} \end{cases} \quad (24)$$

where ϕ, θ and ψ are roll, pitch, and heading, r_1^f represents the displacement of the foot when taking the first step as estimated by Foot-INS.

Since all the evaluated schemes are relative positioning methods, we aligned the initial 10-meter segment of each test trajectory with the reference trajectory. This alignment process ensures consistent initialization of position and heading across the different schemes being compared. It provides a standardized starting point for evaluating their performance in terms of accuracy and reliability.

B. Test results in the office building

In this section, the test trajectories were conducted in an office building corridor scene to evaluate the positioning performance of the proposed method in environments with frequent magnetic interference. Specifically, we conducted 6 tests in a typical office scenario, with 2 testers collecting test data for 3 trajectories each. This setup allows for comprehensive assessment of how well the proposed method performs under realistic indoor conditions where magnetic disturbances are common.

Figure 5 shows 4 test trajectories estimated using 5 positioning schemes in the office building. L-Foot and R-Foot do not provide accurate test trajectories across all tests due to insufficient heading observation information. Dual-Foot improves relative heading observability by using the shortest distance constraint between both feet (L-Foot and R-Foot). However, absolute heading remains unobservable, and it only shows better positioning performance in the fourth test trajectory. Heading-Step addresses the low accuracy issue in traditional step-model PDR by incorporating heading estimation from a quasi-static magnetic field. However, due to frequent magnetic interference in office scenarios, the criteria for identifying quasi-static magnetic fields are strict, resulting in infrequent corrections to heading. As a result, Heading-Step achieves good positioning accuracy only in the second test trajectory. The proposed method demonstrates excellent direction and distance estimation across 4 test trajectories. The estimated trajectories closely match the reference trajectory, indicating the highest positioning accuracy among all schemes evaluated.

Figure 6 shows the cumulative density function (CDF) of position errors for five positioning schemes. The proposed method demonstrates stable positioning performance, with errors distributed within 4 meters across all sampling points in the four tests. Table II presents statistics on the root mean

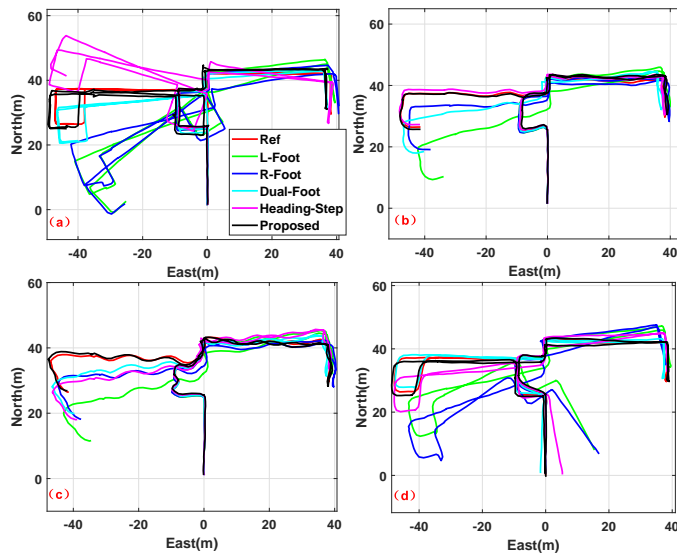


Fig. 5. 4 test trajectories estimated using 5 positioning schemes in the office building.

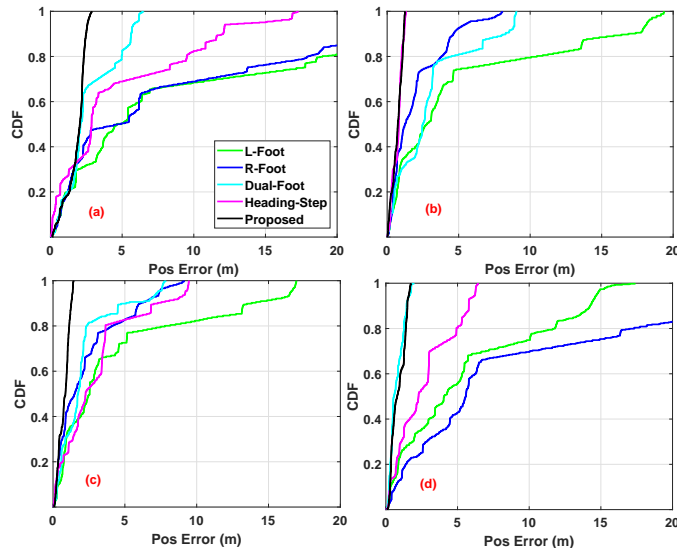


Fig. 6. The cumulative density function of position errors for five positioning schemes in the office building.

square (RMS), 68%, and 95% of position errors for six test trajectories. The RMS averages for L-Foot, R-Foot, Dual-Foot, Heading-Step, and Proposed are 8.56m, 6.63m, 2.71m, 4.06m, and 1.24m, respectively. Compared to L-Foot, R-Foot, and Dual-Foot, the proposed method reduces positioning errors by 85.5%, 81.3%, and 54.3%, respectively. This significant improvement is attributed to the proposed method's utilization of magnetic field vectors within a time window to construct a reliable heading constraint, unaffected by sensor errors and pedestrian dynamics. By addressing the challenge of unobservable absolute heading, the proposed method achieves substantial performance gains. Furthermore, the proposed method reduces position errors by 69.4% compared to Heading-Step, showcasing its robustness against magnetic interference. Leveraging similarities in magnetic field interference within

local spaces, the differential magnetic field vector method effectively mitigates magnetic interference on the compass. In contrast, Heading-Step often fails due to stringent conditions required for judging quasi-static magnetic fields in office scenarios. Therefore, the proposed method excels in reliably correcting heading using magnetic field vectors.

C. Test results in the underground parking lots

Unlike office buildings where magnetic interference originates from the building structure, underground parking lots present another typical scenario with frequent magnetic interference, primarily from parked or moving vehicles. Moreover, pedestrian dynamics in this setting are more natural, as they are less influenced by spatial structures. Therefore, this scenario provides a more comprehensive evaluation of the positioning performance of the proposed method. We conducted six tests in a typical underground parking scenario, with two testers collecting test data for three trajectories each.

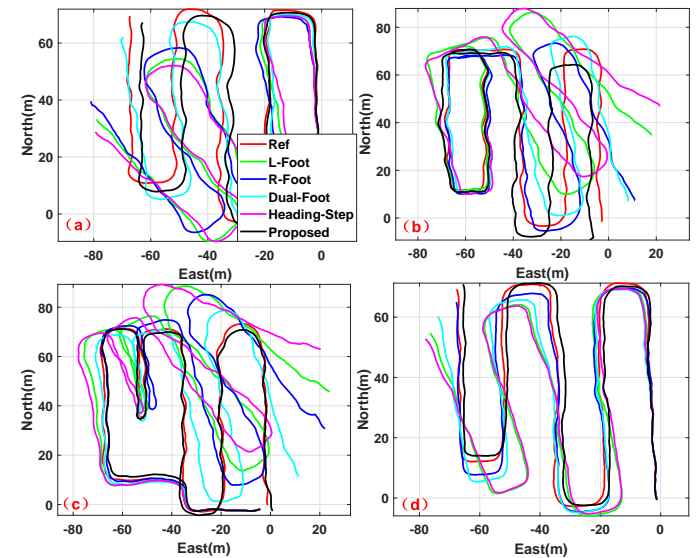


Fig. 7. 4 test trajectories estimated using 5 positioning schemes in the underground parking lots.

Figure 7 shows four test trajectories estimated using five positioning schemes in the underground parking scenario. The proposed method consistently achieves more accurate estimation of all test trajectories compared to other schemes, demonstrating its feasibility and high stability. Sub-figures (a) and (b) reveal noticeable distance errors in the test trajectories estimated by the proposed method. This discrepancy may arise from obstacles on the pavement causing gait deviations, where natural movements of the tester can disrupt the consistent incremental positioning between the foot and waist.

Figure 8 shows the CDF of the position error for five positioning schemes. Table III provides statistics on the RMS, 68%, and 95% position errors for six test trajectories. The RMS average position errors for L-Foot, R-Foot, Dual-Foot, Heading-Step, and Proposed are 12.48m, 6.46m, 5.73m, 15.25m, and 2.92m, respectively. The proposed method reduces positioning errors by 76.6%, 54.8%, 49.0%, and 80.9% compared to other methods, respectively. Heading-Step failed

TABLE II
THE RMS, 68%, AND 95% OF THE POSITION ERRORS IN THE OFFICE BUILDINGS

Test	L-Foot (m)			R-Foot (m)			Dual-Foot (m)			Heading-Step (m)			Proposed (m)		
	RMS	68%	95%	RMS	68%	95%	RMS	68%	95%	RMS	68%	95%	RMS	68%	95%
1	12.91	9.76	28.36	12.01	9.20	27.16	3.25	2.87	5.92	6.60	4.43	14.56	1.93	2.22	2.60
2	7.75	4.13	18.19	2.73	2.06	5.68	3.99	3.15	8.90	0.80	0.91	1.24	0.79	0.94	1.19
3	6.80	4.39	16.56	3.30	2.66	7.40	2.90	2.09	7.31	3.98	3.45	9.21	0.86	1.01	1.37
4	7.50	5.74	14.71	11.15	8.33	22.29	0.89	1.03	1.70	3.30	3.02	6.23	0.99	1.26	1.62
5	7.38	4.45	16.68	7.42	4.98	17.10	3.82	2.66	8.27	10.71	7.35	24.06	1.61	1.99	3.02
6	10.44	9.85	20.07	9.46	8.94	18.40	3.08	3.07	5.67	6.05	5.86	11.19	1.75	1.87	3.00
Mean	8.56	5.95	18.65	6.63	5.15	14.14	2.71	2.33	5.60	4.06	3.49	8.08	1.24	1.46	1.99

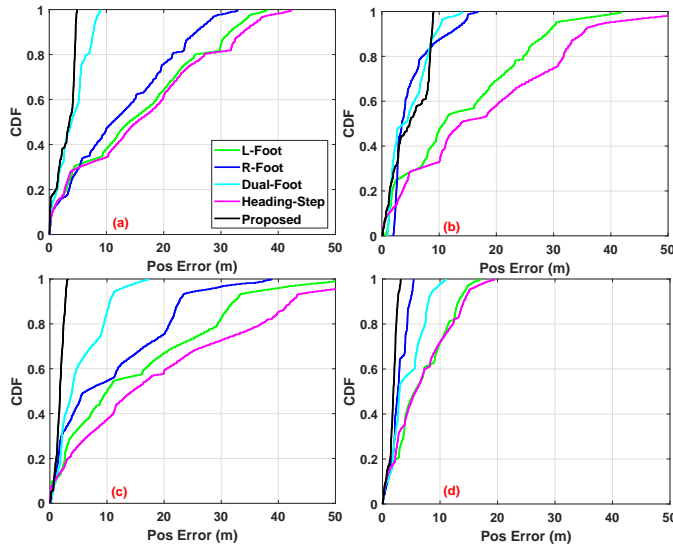


Fig. 8. The cumulative density function of position errors for five positioning schemes in the underground parking lots.

to detect a quasi-static magnetic field in all tests, resulting in significant heading drift. In contrast, the proposed method effectively suppresses magnetic interference without requiring a complex interference detection mechanism, ensuring adaptability across different environments.

In the sixth test, the positioning error of R-Foot is smaller than that of the proposed algorithm. This discrepancy is attributed to very minimal gyroscope bias in this particular test, effectively suppressing position errors caused by heading drift. Although the proposed method achieves stable heading estimation, the assumption of consistent relative position increments between the foot and waist remains vulnerable to disruption by natural human body movements. Despite this, in a statistical sense, positioning errors caused by natural gait patterns are still significantly smaller with the proposed method, outweighing the benefits of improved heading estimation accuracy.

D. Analysis of magnetic interference effects

Using magnetometer observations to provide heading constraints for positioning algorithms in indoor environments necessitates addressing two key challenges: magnetometer bias correction and magnetic interference suppression. The proposed algorithm treats the magnetometer bias as an unknown

state parameter to be estimated, thus eliminating the need for users to actively participate in the correction process. By leveraging the slow variations in magnetic interference within local spaces and the gradual movement of pedestrians, the algorithm constructs a relative constraint of the magnetic vector within a sliding window. This effectively suppresses the influence of magnetic interference, ensuring more accurate and reliable heading constraints for indoor positioning.

Figure 9 illustrates the heading based on magnetic observations, as well as the heading and magnetometer bias estimated by the proposed method in an underground parking lot. 'mHeading' represents the heading estimated from magnetometer observations after subtracting the post-estimated magnetometer bias, while 'gHeading' indicates the heading estimated by the proposed method. As shown in Figure 9-(b), the heading error caused by environmental magnetic interference is 9.96° (RMS), with a maximum error of 31.85° . In contrast, the heading error estimated by the proposed method is 2.21° (RMS), with a maximum error of 5.42° , reflecting a reduction of 77.81% and 82.98%, respectively. Figure 9-(c) shows that the magnetometer biases for the x-axis and y-axis quickly converge to stable estimated values, while the z-axis bias exhibits noticeable fluctuations. This can be attributed to the fact that the plane formed by the x-axis and y-axis is nearly parallel to the plane on which the user walks, allowing sufficient dynamic maneuvers to refine the bias estimation for these axes. The z-axis, however, lacks similar conditions due to the user's complex trajectory. Despite this, the residual magnetometer bias does not significantly impact the accuracy of the heading estimation.

The above results demonstrate that the proposed method effectively suppresses magnetic interference in typical indoor environments (e.g., office and underground parking lot). This success is primarily due to the positive correlation between magnetic field attenuation and the cubic power of the distance. Consequently, the influence range of small-scale magnetic interference is very limited (e.g., less than 1.5 meters [33]), while large-scale magnetic interference exhibits slow regional changes. In typical indoor environments, pedestrians usually do not move close to the wall, so the magnetic field changes at the waist are relatively gentle, which ensures that the assumptions of the proposed method are valid. However, the proposed method may encounter challenges in environments with a high concentration of ferromagnetic materials, such as taking elevators and escalators, and industrial scenes such as

TABLE III
THE RMS, 68%, AND 95% OF THE POSITION ERRORS IN THE UNDERGROUND PARKING LOTS

Test	L-Foot (m)			R-Foot (m)			Dual-Foot (m)			Heading-Step (m)			Proposed (m)		
	RMS	68%	95%	RMS	68%	95%	RMS	68%	95%	RMS	68%	95%	RMS	68%	95%
1	18.85	21.15	34.00	15.50	18.07	28.06	4.74	5.36	8.10	20.15	21.92	36.40	3.35	4.28	4.65
2	17.39	19.41	30.42	6.28	5.03	14.38	5.78	6.72	10.39	22.21	25.08	39.43	5.87	8.06	8.87
3	19.70	20.66	37.38	14.21	15.66	26.66	6.46	6.69	11.74	25.33	25.20	48.28	1.89	2.14	2.82
4	8.11	9.46	14.39	3.15	3.89	5.23	5.07	5.97	8.86	8.46	9.09	15.11	1.95	2.22	2.93
5	6.14	6.55	11.70	6.58	6.90	12.45	6.08	7.26	10.32	10.69	12.32	18.65	2.56	3.09	4.18
6	11.74	12.22	21.83	2.53	2.75	4.51	6.52	7.58	10.67	12.26	12.34	22.22	3.32	3.81	5.08
Mean	12.48	13.63	22.84	6.46	6.87	12.11	5.73	6.55	9.94	15.25	16.36	27.51	2.92	3.53	4.40

power plants. Future work will involve testing the positioning performance in such scenarios to further evaluate and refine the proposed method.

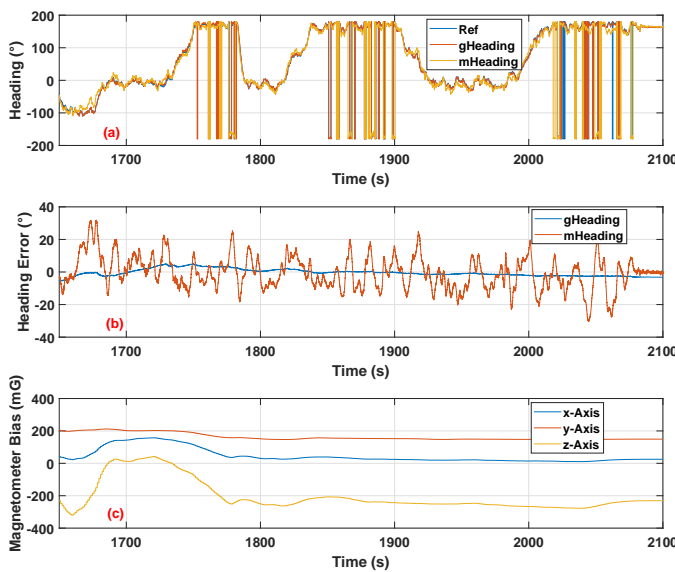


Fig. 9. The heading based on magnetic observations and the heading and magnetometer bias estimated by the proposed method in an underground parking lot. (a) Heading, (b) Heading error, (c) Estimated magnetometer bias.

VI. CONCLUSIONS AND FUTURE WORK

This paper proposes a pedestrian dead reckoning method based on foot-mounted and waist-mounted IMUs with magnetic vector constraints. To address the challenge posed by the dynamic differences between the foot and waist, the paper utilizes relative displacement estimated by Foot-INS to correct the waist-mounted INS. This correction leverages the consistent relative displacement observed when the foot touches the ground twice. Additionally, to mitigate the issue of limited compass availability due to magnetic interference in typical indoor environments, the paper introduces a method based on magnetic vector relative change constraints using a State Cloning Extended Kalman Filter. This approach exploits the similar characteristics of magnetic interference within small local spaces to impose a reliable heading constraint unaffected by significant magnetic interference. The effectiveness of the proposed method was evaluated through 12 tests conducted in typical indoor scenarios such as offices and underground parking lots. Results demonstrate that the

proposed method achieves superior positioning performance compared to existing methods by leveraging magnetic vector constraints, reducing positioning errors by more than 49% compared to single and dual Foot-INS approaches.

The proposed method can provide reliable position estimation during normal walking, but may fail in complex pedestrian movements such as climbing, running, and jumping. In the future, we will try to integrate advanced intelligent algorithms such as deep learning and reinforcement learning into the proposed algorithm to achieve accurate estimation of pedestrian movement positions in complex gait patterns and complex environments. In addition, we will optimize the computational efficiency of the proposed method to meet the needs of real-time pedestrian positioning, and improve its adaptability and positioning performance in embedded systems.

REFERENCES

- [1] A. F. G. G. Ferreira, D. M. A. Fernandes, A. P. Catarino, and J. L. Monteiro, "Localization and positioning systems for emergency responders: A survey," *IEEE Communications Surveys & Tutorials*, vol. 19, no. 4, pp. 2836–2870, 2017.
- [2] N. El-Sheimy and Y. Li, "Indoor navigation: State of the art and future trends," *Satellite Navigation*, vol. 2, no. 1, p. 7, 2021.
- [3] Q. Wang, H. Luo, J. Wang, L. Sun, Z. Ma, C. Zhang, M. Fu, and F. Zhao, "Recent advances in pedestrian navigation activity recognition: A review," *IEEE Sensors Journal*, vol. 22, no. 8, pp. 7499–7518, 2022.
- [4] L. Qi, Y. Liu, Y. Yu, L. Chen, and R. Chen, "Current status and future trends of meter-level indoor positioning technology: A review," *Remote Sensing*, vol. 16, no. 2, p. 398, 2024.
- [5] T. Shan, B. Englot, D. Meyers, W. Wang, C. Ratti, and D. Rus, "Lio-sam: Tightly-coupled lidar inertial odometry via smoothing and mapping," in *2020 IEEE/RSJ international conference on intelligent robots and systems (IROS)*. IEEE, 2020, pp. 5135–5142.
- [6] T. Qin, P. Li, and S. Shen, "Vins-mono: A robust and versatile monocular visual-inertial state estimator," *IEEE transactions on robotics*, vol. 34, no. 4, pp. 1004–1020, 2018.
- [7] T. Liu, J. Kuang, Y. Li, and X. Niu, "A novel minimum distance constraint method enhanced dual-foot-mounted inertial navigation system for pedestrian positioning," *IEEE Internet of Things Journal*, 2023.
- [8] Y. Wang, J. Kuang, X. Niu, and J. Liu, "Llio: Lightweight learned inertial odometer," *IEEE Internet of Things Journal*, vol. 10, no. 3, pp. 2508–2518, 2022.
- [9] J. Kuang, X. Niu, and X. Chen, "Robust pedestrian dead reckoning based on mems-imu for smartphones," *Sensors*, vol. 18, no. 5, p. 1391, 2018.
- [10] Y. Wang, J. Kuang, Y. Li, and X. Niu, "Magnetic field-enhanced learning-based inertial odometry for indoor pedestrian," *IEEE Transactions on Instrumentation and Measurement*, vol. 71, pp. 1–13, 2022.
- [11] J. Chen, B. Zhou, S. Bao, X. Liu, Z. Gu, L. Li, Y. Zhao, J. Zhu, and Q. Li, "A data-driven inertial navigation/bluetooth fusion algorithm for indoor localization," *IEEE Sensors Journal*, vol. 22, no. 6, pp. 5288–5301, 2022.
- [12] Q. Guo, M. Xia, D. Yan, J. Wang, C. Shi, Q. Wang, and T. Li, "Motion pattern recognition for indoor pedestrian altitude estimation based on inertial sensor," *IEEE Sensors Journal*, 2024.

- [13] E. Foxlin, "Pedestrian tracking with shoe-mounted inertial sensors," *IEEE Computer graphics and applications*, vol. 25, no. 6, pp. 38–46, 2005.
- [14] J.-O. Nilsson, D. Zachariah, I. Skog, and P. Händel, "Cooperative localization by dual foot-mounted inertial sensors and inter-agent ranging," *EURASIP Journal on Advances in Signal Processing*, vol. 2013, pp. 1–17, 2013.
- [15] X. Niu, T. Liu, J. Kuang, Q. Zhang, and C. Guo, "Pedestrian trajectory estimation based on foot-mounted inertial navigation system for multistory buildings in postprocessing mode," *IEEE Internet of Things Journal*, vol. 9, no. 9, pp. 6879–6892, 2021.
- [16] C.-S. Jao, A. A. Abdallah, C. Chen, M.-W. Seo, S. S. Kia, Z. M. Kassas, and A. M. Shkel, "Pindoc: Pedestrian indoor navigation system integrating deterministic, opportunistic, and cooperative functionalities," *IEEE Sensors Journal*, vol. 22, no. 14, pp. 14 424–14 435, 2022.
- [17] A. R. Jiménez, F. Seco, F. Zampella, J. C. Prieto, and J. Guevara, "Improved heuristic drift elimination (ihde) for pedestrian navigation in complex buildings," in *2011 International Conference on Indoor Positioning and Indoor Navigation (IPIN)*, 2011, pp. 1–8.
- [18] A. R. Jiménez, F. Seco, J. C. Prieto, and J. Guevara, "Indoor pedestrian navigation using an ins/ekf framework for yaw drift reduction and a foot-mounted imu," in *2010 7th workshop on positioning, navigation and communication*. IEEE, 2010, pp. 135–143.
- [19] I. Skog, J.-O. Nilsson, D. Zachariah, and P. Händel, "Fusing the information from two navigation systems using an upper bound on their maximum spatial separation," in *2012 International Conference on Indoor Positioning and Indoor Navigation (IPIN)*, 2012, pp. 1–5.
- [20] Y. Wu, J. Kuang, and X. Niu, "Wheel-ins2: Multiple mems imu-based dead reckoning system with different configurations for wheeled robots," *IEEE Transactions on Intelligent Transportation Systems*, vol. 24, no. 3, pp. 3064–3077, 2023.
- [21] M. Zhu, Y. Wu, and S. Luo, "Pimu-r: Pedestrian navigation by low-cost foot-mounted dual imus and interfoot ranging," *IEEE Transactions on Control Systems Technology*, vol. 30, no. 1, pp. 247–260, 2022.
- [22] C.-S. Jao, Y. Wang, and A. M. Shkel, "Pedestrian inertial navigation system augmented by vision-based foot-to-foot relative position measurements," in *2020 IEEE/ION Position, Location and Navigation Symposium (PLANS)*, 2020, pp. 900–907.
- [23] Q. Wang, M. Cheng, A. Noureldin, and Z. Guo, "Research on the improved method for dual foot-mounted inertial/magnetometer pedestrian positioning based on adaptive inequality constraints kalman filter algorithm," *Measurement*, vol. 135, pp. 189–198, 2019.
- [24] X. Niu, Y. Li, J. Kuang, and P. Zhang, "Data fusion of dual foot-mounted imu for pedestrian navigation," *IEEE Sensors Journal*, vol. 19, no. 12, pp. 4577–4584, 2019.
- [25] T. Liu, J. Kuang, Y. Li, and X. Niu, "A novel minimum distance constraint method enhanced dual-foot-mounted inertial navigation system for pedestrian positioning," *IEEE Internet of Things Journal*, vol. 10, no. 19, pp. 16931–16944, 2023.
- [26] C. Tjhai and K. OKeefe, "Using step size and lower limb segment orientation from multiple low-cost wearable inertial/magnetic sensors for pedestrian navigation," *Sensors*, vol. 19, no. 14, 2019.
- [27] J. Li, X. Liu, Z. Wang, H. Zhao, T. Zhang, S. Qiu, X. Zhou, H. Cai, R. Ni, and A. Cangelosi, "Real-time human motion capture based on wearable inertial sensor networks," *IEEE Internet of Things Journal*, vol. 9, no. 11, pp. 8953–8966, 2022.
- [28] M. Ma, Q. Song, Y.-h. Li, Y. Gu, and Z.-m. Zhou, "A heading error estimation approach based on improved quasi-static magnetic field detection," in *2016 International Conference on Indoor Positioning and Indoor Navigation (IPIN)*. IEEE, 2016, pp. 1–8.
- [29] T. Michel, P. Genevès, H. Fourati, and N. Layaïda, "On attitude estimation with smartphones," in *2017 IEEE International Conference on Pervasive Computing and Communications (PerCom)*, 2017, pp. 267–275.
- [30] X. Niu, T. Liu, J. Kuang, and Y. Li, "A novel position and orientation system for pedestrian indoor mobile mapping system," *IEEE Sensors Journal*, vol. 21, no. 2, pp. 2104–2114, 2020.
- [31] J. Kuang, X. Niu, and X. Chen, "Robust pedestrian dead reckoning based on mems-imu for smartphones," *Sensors*, vol. 18, no. 5, p. 1391, 2018.
- [32] Y. Wu, D. Zou, P. Liu, and W. Yu, "Dynamic magnetometer calibration and alignment to inertial sensors by kalman filtering," *IEEE Transactions on Control Systems Technology*, vol. 26, no. 2, pp. 716–723, 2017.
- [33] J. Kuang, T. Li, Q. Chen, B. Zhou, and X. Niu, "Consumer-grade inertial measurement units enhanced indoor magnetic field matching positioning scheme," *IEEE Transactions on Instrumentation and Measurement*, vol. 72, pp. 1–14, 2023.



Jian Kuang received the B.Eng. and Ph.D. degrees in geodesy and survey engineering from Wuhan University, Wuhan, China, in 2013 and 2019, respectively. He is currently a Postdoctoral Fellow with the GNSS Research Center, Wuhan University, Wuhan, China. His research interests include inertial navigation, pedestrian navigation, and indoor positioning.



Tao Liu received the B.S. degree in Geographic Information System from Liaoning Technical University, Fuxin, China, in 2015, and M.S. degree in Surveying and Mapping from Liaoning Technical University, Fuxin, China, in 2018, and Ph.D. degree in Geodesy and Surveying Engineering from Wuhan University, Wuhan, China, in 2022. From 2023 to 2024, he was a research assistant with the GNSS Research Center, Wuhan University, Wuhan, China. He is currently a lecturer at the School of Software, Jiangxi Normal University, Nanchang, China. His

research interests focus on inertial navigation, multi-sensor fusion, IMU-based body sensor network, pedestrian navigation, and indoor positioning.



Yan Wang received the B.Eng. degree in chemical engineering and technology and the M.S. degree in computer applied technology from the China University of Mining and Technology, Xuzhou, China, in 2016 and 2019, respectively. He is currently pursuing the Ph.D. degree with the GNSS Research Center, Wuhan University, Wuhan, China. His research interests focus on indoor navigation, sensor fusion algorithm, and computer vision.



Xianmei Meng got her Ph.D degree from School of Nursing at Naval Medical University, China in 2019, and MN degree from School of Nursing, University of Calgary, Canada, in 2008. She is now an assistant professor of Nursing School at Wuhan University in China. Her major research interests are community health nursing and rehabilitation nursing. Dr. Meng has published more than 30 academic papers(one is in a TOP journal), and owned 3 patents.



Xiaoji Niu received the B.Eng. degree (with honors) in mechanical and electrical engineering, and the Ph.D. degree from Tsinghua University, Beijing, China. He was a Post-Doctoral Fellow with the Mobile MultiSensor Systems (MFMSS) Research Group, Department of Geomatics Engineering, University of Calgary. He was also a Senior Scientist with SiRF Technology, Inc. He is currently a Professor with the GNSS Research Center and the Collaborative Innovation Center of Geospatial Technology, Wuhan University, Wuhan, China. His

research interests include INS and GNSS/INS integration for land vehicle navigation and pedestrian navigation.